ACS APPLIED MATERIALS & INTERFACES

Research Article

www.acsami.org

Laser Printing of Nanoparticle Toner Enables Digital Control of Micropatterned Carbon Nanotube Growth

Erik S. Polsen,[†] Adam G. Stevens,[†] and A. John Hart*

Mechanosynthesis Group, Department of Mechanical Engineering, University of Michigan, 2350 Hayward Street, Ann Arbor, Michigan 48109

Supporting Information

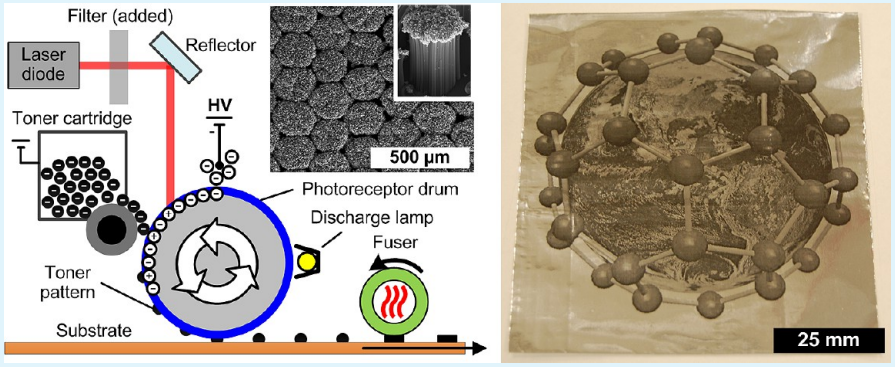

ABSTRACT: Commercialization of materials utilizing patterned carbon nanotube (CNT) forests, such as hierarchical composite structures, dry adhesives, and contact probe arrays, will require catalyst patterning techniques that do not rely on cleanroom photolithography. We demonstrate the large scale patterning of CNT growth catalyst via adaptation of a laser-based electrostatic printing process that uses magnetic ink character recognition (MICR) toner. The MICR toner contains iron oxide nanoparticles that serve as the catalyst for CNT growth, which are printed onto a flexible polymer (polyimide) and then transferred to a rigid substrate (silicon or alumina) under heat and mechanical pressure. Then, the substrate is processed for CNT growth under an atmospheric pressure chemical vapor deposition (CVD) recipe. This process enables digital control of patterned CNT growth via the laser intensity, which controls the CNT density; and via the grayscale level, which controls the pixelation of the image into arrays of micropillars. Moreover, virtually any pattern can be designed using standard software (e.g., MS Word, AutoCAD, etc.) and printed on demand. Using a standard office printer, we realize isolated CNT microstructures as small as 140 μm and isolated catalyst "pixels" as small as 70 μm (one grayscale dot) and determine that individual toner microparticles result in features of approximately 5−10 μm . We demonstrate that grayscale CNT patterns can function as dry adhesives and that large-area catalyst patterns can be printed directly onto metal foils or transferred to ceramic plates. Laser printing therefore shows promise to enable high-speed micropatterning of nanoparticle-containing thin films under ambient conditions, possibly for a wide variety of nanostructures by engineering of toners containing nanoparticles of desired composition, size, and shape.

KEYWORDS: *carbon nanotubes, laser printing, electrostatic, manufacturing, nanoparticles, adhesive*

High-speed printing technologies, including letterpress, inkjet, and imprint methods are used widely for patterning consumer products ranging from plastic bags to flash memory.[1,2] Industrialization of printing has been enabled both by innovations in the formulation of inks, as well as in the printing method and machine technology. The growing availability of chemically synthesized nanostructures such as semiconductor, oxide, and polymer particles, indicates potential for adopting printing technology to manufacturing of patterned nanostructured materials. Nevertheless, most research on fabrication of nanostructured thin films still leverages photolithography methods, and it remains an important need to invent scalable methods for patterning nanostructures, which combine engineerable control of feature size and density with high throughput.

Moreover, printing methods that are compatible with low-cost desktop machines, such as inkjet and laser printers, offer promise for customized materials design and fabrication, and their integration with traditional microfabrication and thin film lamination technologies. Laser printing has been used to fabricate microfluidic devices where the toner either defined the thickness and width of the channels, on both polymer and paper substrates,[3] or where the toner defined a wet chemical

Received: January 13, 2013
Accepted: February 25, 2013
Published: February 25, 2013

mask for the creation of microfluidic devices in glass.[4] The scalability and accessibility of this is particularly attractive for paper-based point-of-care diagnostic devices, originally envisioned by Martinez et al.[5] The basic principle of laser printing—electrostatic attraction of charged particles to a surface—has also been adapted for direct patterning of nanoparticle clusters.[6]

Much like microfluidic devices, several applications of vertically aligned CNT (VACNT) forests such as, hierarchical composite structures,[7] dry adhesives,[8] and contact probe arrays,[9] require large-area patterning methods to become commercially viable. The deposition of patterned catalysts for CNT growth traditionally involves vacuum deposition methods combined with batch-style photolithography.[10] Inkjet printing has been used to print CNT catalyst and a wide variety of other nanoparticle solutions, but the wetting of the liquid and the drying kinetics of the solution can limit the uniformity and minimum feature size of the resulting patterns.[11] Microcontact printing has also been applied to pattern catalyst solutions for subsequent growth of CNT forests.[12,13] Additionally, deposition of metal-loaded block copolymers can control the diameter and areal density of CNTs, and this method has been implemented by spin-coating as well as microcontact printing.[14,15] However, use of these techniques in a continuous fashion and/or over large scales requires specialized equipment, and in the case of contact printing methods replacement of the soft stamp may be required. Thus, there remains a need for a highly flexible and scalable method for patterning nanoparticle catalyst for CNT manufacturing on alternative (e.g., flexible/metallic) and large-area substrates.

We demonstrate fabrication of nanoparticle-containing micropatterns by laser printing and the use of this technology to engineer the growth of CNT forests and patterned microstructures on substrates. CNT forests grown from toner micropatterns are shown to have comparable CNT diameter, alignment, and density to those grown with standard thin-film catalysts. Additionally, large-area micropillar arrays with prescribed density can be made simply by adjusting the grayscale contour, down to a minimum catalyst pixel size of 70 μm (one grayscale dot) using a standard home/office printer. Last, we show that grayscale micropillar patterns made by this method can be used as compliant dry adhesives and that the process can be scaled up for printing onto metal substrates or large ceramic plates.

RESULTS AND DISCUSSION

Laser Printing of Nanoparticle Toner Micropatterns. Figure 1a illustrates the general method of laser printing, where a laser beam is rastered across a photosensitive drum. This induces a positive charge on the drum surface, which in turn attracts negatively charged toner particles to the appropriate locations. The drum rotates continuously, and the pattern of toner particles is then pressed against, and adheres to, the target substrate, such as a sheet of paper. Heat and pressure applied to the substrate using a set of contacting rollers causes the toner particles to soften and adhere. This also forms continuous dot features on the paper, by coalescence of groups of particles that were attracted to the same focal spot of the laser.

We found that a low-cost home/office laser printer (Figure 1b) is capable of patterning microscale toner features containing metal nanoparticles, with feature size limited by the laser spot size and toner particle size. Specifically, we studied the printing of commercially available magnetic ink

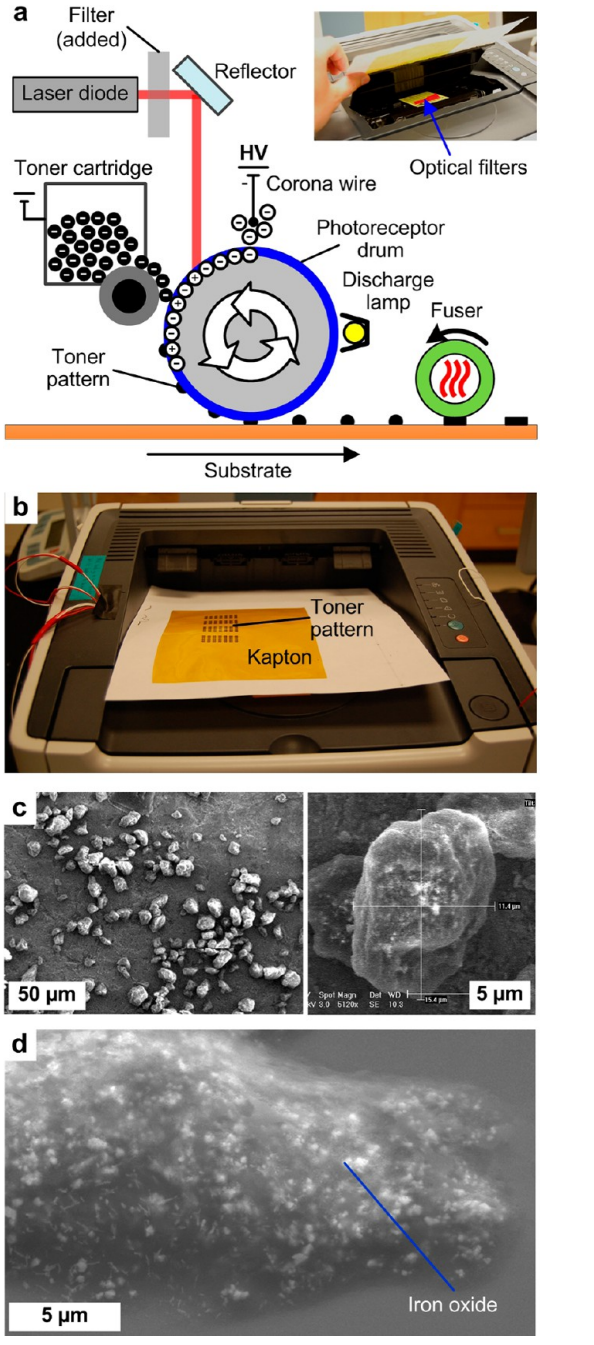

Figure 1. Modified laser printing for large-area manufacturing of micropatterns with nanoparticle toner: (a) schematic of laser printer mechanism, indicating placement of filter for modulation of laser intensity; (b) printer during operation with Kapton substrate; (c) SEM images of individual MICR toner particles harvested from cartridge; (d) printed toner particle, where high contrast dots are iron oxide nanoparticles.

character recognition (MICR) toner, which is widely used throughout the financial industry to enable the electronic processing of checks. The magnetic properties of the printed toner are established by inclusion of iron oxide particles within the toner,[16] and the wide usage of this toner in industry has driven the compatibility with most office printers. However, to our knowledge the details of the particles within this toner have not been studied previously in the context of micro/nanofabrication research.

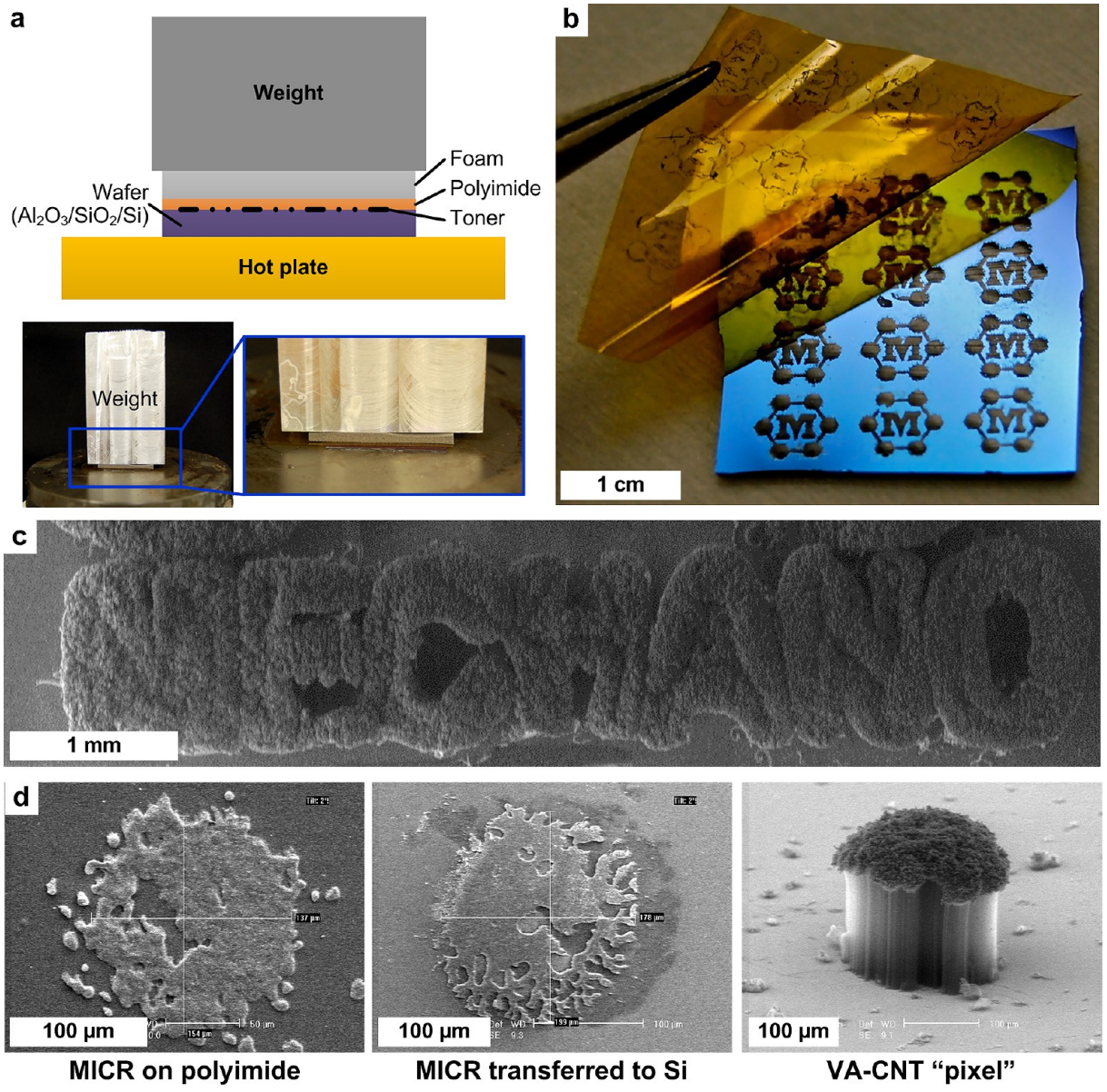

Figure 2. Thin-film transfer process and resulting micropatterns: (a) schematic and photograph of transfer setup; (b) removal of Kapton substrate, leaving nanoparticle micropatterns behind; (c) top view of "MECHANO" after CNT growth, where the pattern was created by laser printing of 2 point font; (d) individual 2 point "." characters at each stage of the process.

Toner used in this study (Figure 1c and d) was purchased as a sealed cartridge for use in the printer (micrpro.com, HP Q7553X), and by SEM imaging, we determined that the toner microparticles have irregular shapes and are roughly 10−20 μm wide. By thermogravimetric analysis (TGA, Supporting Information Figure S1), we determined that the toner contains approximately 40% polymer, which thermally decomposes below 500 °C; the remnants are carbon black (to provide optical contrast), and iron oxide (to impart magnetic read properties).

Because iron nanoparticles are used widely as the catalyst for CNT growth, we studied the applicability of MICR laser printing for direct-write manufacturing of catalyst patterns for CNT growth. To fabricate the patterns, we first designed the pattern using computer software (AutoCAD), printed the pattern onto a polyimide (Kapton) substrate using the laser printer, and then transferred the pattern to an oxide-coated silicon wafer, completing preparation for subsequent CNT growth using a standard thermal chemical vapor deposition (CVD) process (Supporting Information Figure S2). Because laser printing on paper deposits many layers of toner particles in order to achieve high optical contrast, we made one modification to the printer to reduce the amount of toner deposited. A series of neutral density filters (each with 50% transmission) were installed between the laser diode and the photosensitive drum (Figure 1b). The filters therefore reduced the charge density on the drum by reducing the laser intensity incident upon the drum. This enabled control of the density of toner particles independently from the design of the printed image and grayscale level. While patterns could be created using any software, use of CAD software facilitated comparison of the designed pattern with the dimensions of the features at each stage of the process.

Pattern Transfer. After printing, the MICR pattern on the polyimide sheet was transferred to a silicon wafer for CNT synthesis. The polyimide was placed toner-down on a wafer

that had been coated with 10 nm Al_2O_3 (Figure 2a); this alumina support layer stabilizes the catalyst particles against agglomeration at high temperature and influences CNT nucleation and growth.[17] A layer of silicone foam was placed on top of the inverted polyimide film, followed by an aluminum block which due to its weight exerted a uniform pressure of approximately 180 kPa. This stack was placed on a hot plate preheated to 150 °C for 6 s. After removing the heat source and the pressure and letting the stack cool to room temperature (approximately 1 min), the Kapton was manually peeled back from the silicon substrate, leaving behind the patterned toner (Figure 2b). As discussed in further detail later, the patterned image transferred to the silicon wafer results in patterned CNT growth via a standard atmospheric pressure thermal CVD recipe (see Experimental Methods), such as the example word "MECHANO" in Figure 2c.

SEM imaging of single dots "." characters, 2 point font size) before and after the transfer process revealed that the area of the printed pattern increases by 60% due to the reflow of the melted toner under pressure (Figure 2d). These features are approximately 140 and 190 μm wide, respectively, and are patchy due to the nonuniform distribution of the toner which is easily seen at this high magnification. The transferred patterns result in growth of CNT forest structures ("pixels") of equivalent size, which are interestingly more continuous than the microscale catalyst features due to reflow of the toner at high temperature. Catalyst features as small as 70 μm were printed on Kapton, but these did not uniformly transfer to the silicon wafer. Nevertheless, the smallest feature that could potentially be created is limited by the size of the toner particles, and this is much smaller than the smallest feature that is consistently produced by the printer that was used. And, each toner particle still contains thousands of nanoparticles which can yield individual CNTs.

Digital Control of CNT Growth. The same CVD recipe was used to produce CNT forests with scales ranging from centimeter-wide patterns (Figure 2c) to individual dot features (Figure 2d), with heights controllable by the growth time. However, due to the excess quantity of nanoparticles and binder in the toner, as well as the polydispersity of the particles, the CNT forest grown from MICR has a dense "crust" on its top surface (Supporting Information Figure S3a). As determined by Raman spectroscopy and TEM (results not shown), this crust comprises amorphous carbon and carbon "onions" which overcoat larger nanoparticles or aggregates that do not grow CNTs. Incidentally, the CNT forest growth directly after transfer to the wafer can be delaminated, and the same substrate can be used to grow a second layer of CNTs without additional catalyst deposition. In this case, a thin layer of catalyst particles is left behind on the wafer, and the resulting second CNT forest has a much flatter top surface (Supporting Information Figure S3b). As is typical in a CNT growth process, the substrate is treated in a reducing atmosphere immediately prior to CNT growth to reduce the iron oxide.[18,19]

The capability to independently adjust the shape and grayscale intensity of the pattern, along with the modification of laser intensity (using the installed features) enables hierarchical control of the CNT forest structure. CNT forests were grown on substrates printed with 25−100% of the nominal laser intensity (0−2 installed filters), and importantly, we found that the laser intensity determined the mass density of the CNT forest (Figure 3d). Therefore, the number of toner particles printed, and therefore the number of active catalyst

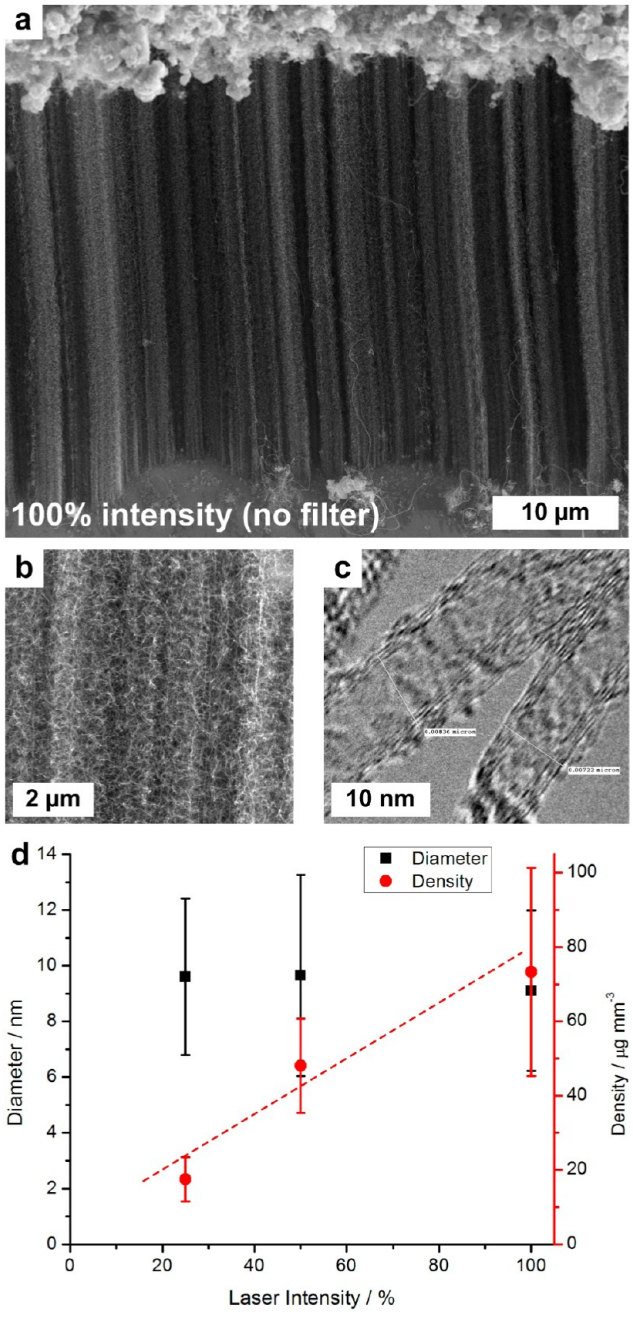

Figure 3. Characterization of CNT forests grown from MICR catalyst nanoparticles: (a) SEM image of CNT forest; (b) magnified SEM image showing CNT tortuosity and density; (c) TEM image of few-walled CNTs from the forest, with indicated diameters approximately 8 and 7 nm; (d) CNT diameter and density statistics versus laser intensity, showing that CNT forest mass density is controlled by the laser intensity, yet CNT diameter distribution is invariant.

nanoparticles for CNT growth, is proportional to the laser intensity. Within the measurement error computed for the three values investigated, a linear trend can be extrapolated. A more precise trend could be obtained via finer control of the laser intensity by direct modulation or using a different series of filters.

We also found that the CNT diameter does not change along with the density. The CNT diameter distribution was quantified using transmission small-angle X-ray scattering (SAXS),[20,21] by fitting linescans of the SAXS images to a

dx.doi.org/10.1021/am400148t | ACS Appl. Mater. Interfaces 2013, 5, 3656−3662

mathematical model of the CNTs as a lognormally distributed population of hollow cylinders. For all intensity levels, the average CNT diameter was 10 ± 2 nm. The diameter statistics were also verified by TEM imaging. The measured variance of ±2 nm is comparable to that achieved by dewetting of thin film catalysts for CNT growth.[22] Therefore, the ability to engineer CNT density by the laser printing intensity does not come at the expense of larger CNT diameter due to agglomeration of the catalyst particles, in spite of the surplus quantity of toner that is printed onto the substrate. Additionally, we expect that control of the catalyst nanoparticle size within the toner would enable control of the CNT diameter.[23]

Moreover, we found that printing of grayscale patterns enabled growth of regularly spaced CNT micropillar arrays, where each grayscale dot led to a single micropillar. This is because a standard printer driver converts a grayscale tone to an equivalent size and density of evenly spaced dots, rather than adjusting the density of the printed toner particles without pixellation. Increasing the grayscale level (i.e., from dark to light) decreases the dot size, thus increasing the white space between dots on the printed page. Optical images of MICR patterns at different grayscale levels are seen in Figure 4a, along with an exemplary array of CNT micropillars growth from the 50% grayscale pattern in Figure 4b. Micropillars grown from a 75% grayscale pattern are also shown in Supporting Information Figure S4, where the additional free space between the pillars and the smaller pillar diameters allow them to tilt. The diameter of each micropillar in the 50% grayscale pattern is approximately 150 μm (Figure 4c), and the micropillars are arranged in a hexagonal lattice pattern. As discussed earlier, this is close to the resolution limit of the present catalyst printing and transfer process. However, at the edges of these patterns, we found much smaller CNT forest features that appear to have grown from stray MICR toner particles. These tall slender forests were found with diameter as small as 5 μm (Figure 4d). This indicates that ultimate resolution of the process will be determined by the size and uniformity of the toner particles, in concert with the resolution of the charge pattern created by the printer mechanism. Therefore, we expect that higher resolution laser printers, which have higher fidelity of charge patterning in the printing mechanism, will allow for printing of higher resolution micropatterns for CNT growth and other applications.

Demonstrations. Previous studies have shown that CNT forests can function as dry adhesives and that patterning of the CNT forests enables control of the interface compliance while maintaining large numbers of micro- and nanoscale contacts.[24,25] Therefore, we hypothesized that the large area uniformity and tunable properties of laser printed arrays would make our material an attractive large-area dry adhesive. An array of microstructures patterned using 50% laser intensity and a grayscale gradient (transitioning from no toner to full black) was fabricated using the same printing, transfer, and CVD process described above. Using finger pressure, the sample was pressed onto a clean glass microscope slide and additional weight was added until the sample detached from the glass (Figure 5a). Before detaching, the sample supported 85 g, which is approximately 1.2 N cm^{-2} overall, and 25 N cm^{-2} based on an estimate of the CNT area in contact with the glass slide. These values are lower than previous reports using CNT forests grown from thin film catalysts (up to 100 N cm^{-2});[8,24] however, we expect that much higher strength could be achieved by engineering the laser-printed growth process to have a thinner top layer, so that a greater number of CNTs contact the glass directly. Additionally, we observe that during compression and detachment some of the CNT micropillars are bent to the side, suggesting that the measured adhesion is determined by contact of the CNTs on the micropillar sidewalls with the glass (Figure 5b, Supporting Information Figure S5).

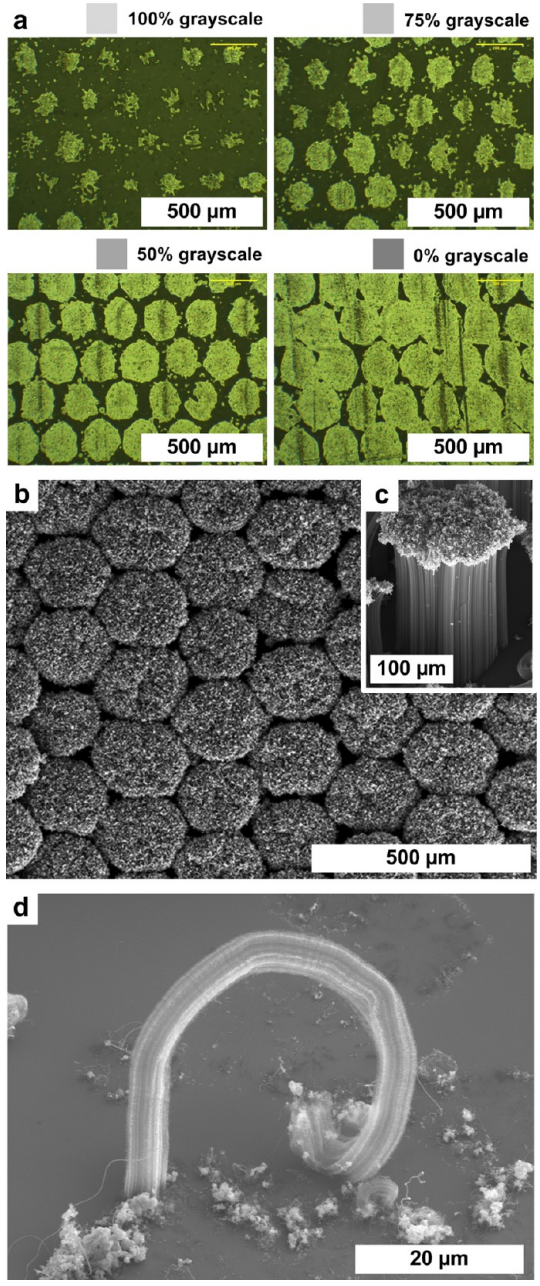

Figure 4. Grayscale-controlled printing of CNT micropillar arrays: (a) optical micrographs of MICR on alumina substrate, showing increasing pattern density with decreasing grayscale lightness (as seen on-screen); (b) SEM image of a an array of CNT micropillars, from a 50% grayscale pattern; (c) SEM image of a single micropillar at the edge of the patttern; (d) small isolated micropillar grown from a single errant toner particle, indicating the potential for increased printing resolution via charge patterning.

Last, we demonstrate the ability to scale the laser printing process to larger areas. An enlarged (100 mm wide) image of the Earth encapsulated by a C60 fullerene was printed directly onto a sheet of aluminum foil as shown in Figure 5c (original

dx.doi.org/10.1021/am400148t | ACS Appl. Mater. Interfaces 2013, 5, 3656−3662

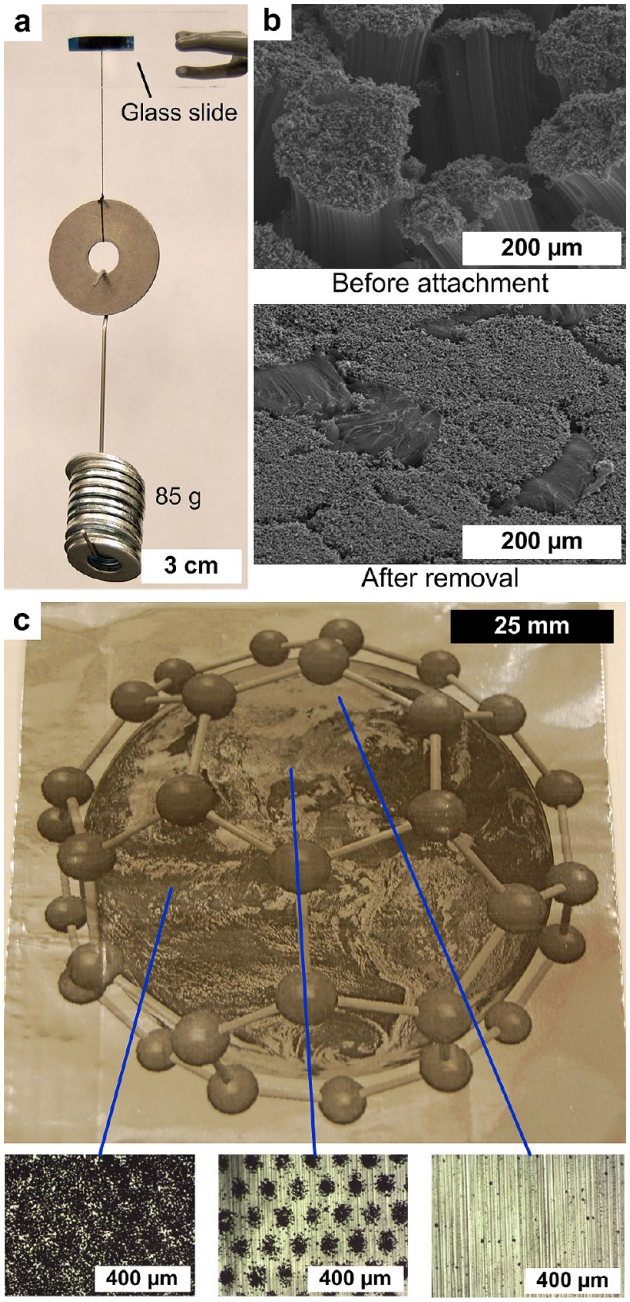

Figure 5. Demonstration of the applicability of MICR printing to dry adhesives and large-area patterning: (a) micropatterned MICR-catalyzed CNT forest supporting load in shear; (b) before/after SEM images of CNT forest used as a dry adhesive, showing resulting forest deformation; (c) large area MICR printing of an image of the Earth encapsulated by a C60 fullerene on an aluminum foil sheet, with optical micrograph close-ups showing grayscale gradients.

image shown in Supporting Information Figure S6). This image contains the full range of grayscale levels, and we verified that the MICR printing and transfer process can accurately reproduce this image. The same pattern was also printed onto polymide and transferred to an alumina plate (Supporting Information Figure S6). This demonstration also emphasizes that the use of Si substrates in the present study was a matter of convenience rather than necessity, and future work will focus on adaptation of the CNT growth recipe for MICR toner patterned on large-area ceramic plates and metal foils. We also found that large-area transferred patterns can exhibit small voids due to entrapment of air beneath the polyimide. Therefore, application of uniform pressure by a roller could enable continuous pattern transfer that is compatible with continuous laser printing of the toner pattern.

CONCLUSIONS

We presented a scalable, cost-effective method for depositing catalyst micropatterns for CNT growth, via laser printing of MICR toner using a conventional office printer. Hierarchical and "digital" control of CNT growth is achieved by programming of the pattern shape, grayscale level (micropillar density), and laser intensity (CNT density). While the minimum feature sizes achieved are significantly greater than the capabilities of optical lithography, use of a high resolution printer and smaller MICR toner particles would enable significantly finer resolution while maintaining the high production rate. This technique is promising for cost-effective fabrication of large-area CNT films, both for patterned and nonpatterned applications, such as dry adhesives, optical absorbers, and mechanical reinforcements. Moreover, the development of new toner formulations containing engineered compositions and sizes of nanoparticles may enable the adoption of laser printing as a scalable nanomanufacturing process for control of CNT diameter and density and for patterning and growth of other nanostructures.

EXPERIMENTAL METHODS

Sample Preparation. A custom pattern was generated using CAD software (SolidWorks) and scaled to the desired dimensions. Kapton film (0.001 in. thick) was mounted to a sheet of 22 lb paper, as a reinforcing layer, with adhesive tape around the perimeter to create the printing substrate. The substrate was loaded into a modified laser printer (Hewlett-Packard 2015DN) that then printed the MICR toner in the pattern dictated by the user file. Neutral density filters (Thorlabs, Model no. NE203B) were optionally placed between the laser and the photoreceptor drum to control the thickness of the deposited toner. After printing, the Kapton sheet was cut from the paper backing with a razor blade and placed toner-down on a substrate that consisted of 10 nm of Al_2O_3 deposited by e-beam evaporation on (100) silicon wafers coated with 300 nm of thermally grown SiO_2. A 5 mm silicone foam layer was placed on top of the Kapton sheet as insulation, and this assembly was transferred to a hot plate (Heidolph MR Hei-Standard) preheated to 150 °C. A mass was then placed on top of the stack resulting in an approximate pressure of 180 kPa, which was applied for 6 s. After cooling to room temperature, the Kapton was peeled back from the substrate, leaving behind the patterned toner.

CNT Growth. CNT growth was performed using a Lindberg Blue M horizontal tube furnace with a 25 mm OD quartz tube (22 mm ID, 300 mm heated length) at atmospheric pressure, with flows of $He/H_2/C_2H_4$ (400/100/100 sccm), at 775 °C for 15 min, preceded by an annealing step at 775 °C for 10 min with flows of 100/400 sccm He/H_2. The samples were rapidly cooled in the growth atmosphere before purging the CVD chamber with He when the thermocouple reading dropped below 250 °C.

Adhesion Testing. Two-part epoxy was used to attach a piece of thread to the back of the grown substrate, and the other end of the thread was tied around a washer. Using isopropyl alcohol (IPA), a glass microscope slide was wiped clean and the forest was pressed onto the slide with finger pressure. The slide was then mounted in a ring clamp such that the washer hanging on the thread was loading the sample in shear. A metal hanger was hooked on the washer which allowed additional washers to be added to increase the shear load on the sample. The sample was loaded until failure occurred, and the final stable weight was recorded.

Characterization. Mass measurements of the substrates were collected before and after MICR transfer to the substrate, and again after CNT growth, using an Ohaus Discovery microbalance. The differential between the measurements before and after MICR transfer was multiplied by the percent value of iron oxide in the toner that was obtained through TGA to obtain the mass of the catalyst particles. Subtracting the mass of the catalyst particles, and the mass of the bare substrate, from the sample mass with CNT growth represented the mass of CNTs grown on the substrate. The areal coverage of each VACNT array was calculated using contrast pixel counting in Adobe Photoshop CS6, using images taken by a Nikon D40 camera. SEM imaging was performed using a FEI Nova Nanolab, and forest heights were measured directly from SEM images at different magnifications. The combination of the mass, area, and height measurements was used to calculate the areal and volumetric densities of the VACNT arrays. For X-ray scattering measurements, the CNT forest is placed on a motorized stage in the beampath of the G1 beamline at Cornell High Energy Synchrotron Source (CHESS). A beam energy of 10 ± 0.1 keV (wavelength ≈ 0.13 nm) is selected with synthetic multilayer optics (W/B4C, 27.1 Å d-spacing), and the beam is focused down to ≈20 μm using mechanical slits upstream. The beam size is accurately measured by scanning the beam over a pinhole slit mounted on a motorized stage while measuring the beam intensity. The downstream X-ray intensity measurements are normalized to the upstream measurements in order to eliminate the effect of the drift in synchrotron intensity with time. A standard sample of silver behenate powder (d_{001} = 58.380 Å) is used to calibrate the pixel-to-q ratio. Linescans from the 2D SAXS patterns are fitted using a mathematical model for lognormally distributed hollow cylinders. These scans are obtained by integration of intensities within ±10° from the reference direction (x-axis) of the inverse space parameter q (chosen to be the direction of maximum intensity). The fitting code used an iterative approach in searching for the best fit within a user defined fitting range. By including the low q part of the data, a good fit was achieved that selects a probability density function (PDF) for diameter distribution as well as for the ratio c = ID/OD, where ID is the inner diameter of the multiwalled CNT and OD is the outer diameter of the multiwalled CNT.

■ ASSOCIATED CONTENT

Ⓢ Supporting Information

Additional data and figures as described in the text. This material is available free of charge via the Internet at http://pubs.acs.org.

■ AUTHOR INFORMATION

Corresponding Author

*E-mail: ajohnh@umich.edu.

Author Contributions

†These authors contributed equally to this work.

Notes

The authors declare no competing financial interest.

■ ACKNOWLEDGMENTS

We thank Mostafa Bedewy and Arthur Woll for their assistance with the X-ray scattering data collection and Nicholas A. Kotov for use of the TGA instrument in his laboratory. This work was supported by the Scalable Nanomanufacturing Program of the National Science Foundation (DMR-1120187) and the DoD, Air Force Office of Scientific Research, National Defense Science and Engineering Graduate (NDSEG) Fellowship, 32 CFR 168a awarded to E.S.P. X-ray scattering was performed in the G1 beamline at the Cornell High-Energy Synchrotron Source (CHESS), which is supported by the NSF and the National Institutes of Health under Grant DMR-0225180. Electron microscopy and AFM were performed at the University of Michigan Electron Microbeam Analysis Library (EMAL), and microfabrication was performed at the Lurie Nanofabrication Facility (LNF) which is a member of the National Nanotechnology Infrastructure Network.

■ REFERENCES

(1) Derby, B. *Annu. Rev. Mater. Res.* **2010**, *40*, 395−414.
(2) Schift, H. *J. Vac. Sci. Technol., B: Microelectron. Nano. Struct.* **2008**, *26*, 458.
(3) Coltro, W. K. T.; De Jesus, D. P.; Da Silva, J. A. F.; Do Lago, C. L.; Carrilho, E. *Electrophoresis* **2010**, *31*, 2487−2498.
(4) Coltro, W. K. T.; Piccin, E.; Fracassi da Silva, J. A.; Lucio do Lago, C.; Carrilho, E. *Lab Chip* **2007**, *7*, 931−4.
(5) Martinez, A. W.; Phillips, S. T.; Butte, M. J.; Whitesides, G. M. *Angew. Chem., Int. Ed.* **2007**, *46*, 1318−20.
(6) Barry, C. R.; Steward, M. G.; Lwin, N. Z.; Jacobs, H. O. *Nanotechnology* **2003**, *14*, 1057−1063.
(7) Garcia, E. J.; Wardle, B. L.; John Hart, A. *Compos. Part A: Appl. Sci. Manuf.* **2008**, *39*, 1065−1070.
(8) Qu, L.; Dai, L.; Stone, M.; Xia, Z.; Wang, Z. *Science* **2008**, *322*, 238−242.
(9) Lee, J.; Chandrashekar, A. *Solid-State Sens., Actuators Microsyst.* **2005**, 1943−1946.
(10) Hart, A. J.; Slocum, A. H. *J. Phys. Chem. B* **2006**, *110*, 8250−8257.
(11) Mansoor, M.; Kinloch, I.; Derby, B. *Key Eng. Mater.* **2010**, *442*, 7−14.
(12) Michel, B.; Bernard, a.; Bietsch, a.; Delamarche, E.; Geissler, M.; Juncker, D.; Kind, H.; Renault, J.-P.; Rothuizen, H.; Schmid, H.; et al. *IBM J. Res.Dev.* **2001**, *45*, 697−719.
(13) Bonard, J.-M.; Weiss, N.; Kind, H.; Stöckli, T.; Forró, L.; Kern, K.; Chatelain, A. *Adv. Mater.* **2001**, *13*, 184−188.
(14) Bennett, R. D.; Hart, A. J.; Cohen, R. E. *Adv. Mater.* **2006**, *18*, 2274−2279.
(15) Cassell, A. M.; McCool, G. C.; Ng, H. T.; Koehne, J. E.; Chen, B.; Li, J.; Han, J.; Meyyappan, M. *Appl. Phys. Lett.* **2003**, *82*, 817−819.
(16) Wang, Z.-M.; Wagner, J.; Wall, S. *Aerosol Sci. Technol.* **2011**, *45*, 1060−1068.
(17) Amama, P. B.; Pint, C. L.; Mirri, F.; Pasquali, M.; Hauge, R. H.; Maruyama, B. *Carbon* **2012**, *50*, 2396−2406.
(18) Dupuis, A. *Prog. Mater. Sci.* **2005**, *50*, 929−961.
(19) Wirth, C. T.; Bayer, B. C.; Gamalski, A. D.; Esconjauregui, S.; Weatherup, R. S.; Ducati, C.; Baehtz, C.; Robertson, J.; Hofmann, S. *Chem. Mater.* **2012**, *24*, 4633−4640.
(20) Wang, B. N.; Bennett, R. D.; Verploegen, E.; Hart, A. J.; Cohen, R. E. *J. Phys. Chem. C* **2007**, *111*, 5859−5865.
(21) Meshot, E. R.; Plata, D. L.; Tawfick, S.; Zhang, Y.; Verploegen, E. A.; Hart, A. J. *ACS Nano* **2009**, *3*, 2477−2486.
(22) Bedewy, M.; Meshot, E. R.; Reinker, M. J.; Hart, A. J. *ACS Nano* **2011**, *5*, 8974−8989.
(23) Alvarez, N. T.; Li, F.; Pint, C. L.; Mayo, J. T.; Fisher, E. Z.; Tour, J. M.; Colvin, V. L.; Hauge, R. H. *Chem. Mater.* **2011**, *23*, 3466−3475.
(24) Ge, L.; Sethi, S.; Ci, L.; Ajayan, P. M.; Dhinojwala, A. *Proc. Natl. Acad. Sci. U. S. A.* **2007**, *104*, 10792−5.
(25) Chen, B.; Oppenheimer, P. G.; Shean, T. A. V.; Wirth, C. T.; Hofmann, S.; Robertson, J. *J. Phys. Chem. C* **2012**, *116*, 20047−20053.

■ NOTE ADDED AFTER ASAP PUBLICATION

In the version of this paper published on March 8, 2013, there were issues with permissions for copyrighted material in some of the figures. Those graphics have been changed in this version to resolve the problem. The corrected version was reposted on April 23, 2013.